

# Conductivity influence on interfacial waves in liquid metal batteries and related two-layer systems

T. Weier<sup>1</sup>, I. Grants<sup>2</sup>, G.M. Horstmann<sup>1</sup>, S. Landgraf<sup>1</sup>, M. Nimtz<sup>1</sup>, P. Personnetaz<sup>1</sup>,  
F. Stefani<sup>1</sup>, and N. Weber<sup>1</sup>

<sup>1</sup>Helmholtz-Zentrum Dresden - Rossendorf, Bautzner Landstr. 400, 01328 Dresden, Germany  
<sup>2</sup>Institute of Physics, University of Latvia, Salaspils-1, LV-2169, Latvia

January 28, 2020

## Abstract

Fluid flows in liquid metal batteries can be generated by a number of effects. We start with a short overview of different driving mechanisms and then address questions specific to the metal pad role instabilities in three-layer systems. We focus on the role of the conductivity distribution in the cell, noting at the same time that interfacial tension should be considered as well for smaller cells. Following this discussion, numerical results on the excitation of interfacial waves in two-layer liquid metal systems with miscibility gaps bearing an interface normal electric current are presented. Confirming recent results from the literature, we find that magnetic damping plays a decisive role for strong vertical magnetic fields. In addition, boundary conditions for the electric field strongly influence critical currents and growth rates.

## Introduction

Liquid metal batteries (LMBs) are possible candidates for meeting the large-scale storage demands of future electricity systems relying mainly on volatile sources as wind power and photovoltaics. Single LMB cells contain three liquid layers in stable density stratification: typically an alkaline or earth alkaline metal as the negative electrode (N) on the top, a molten salt mixture as the electrolyte (E) in the middle and a heavy post-transition metal or metalloid at the bottom (P), see Fig. 1a. A comprehensive overview on LMBs including their history is provided by Kim et al. [1].

Due to the molten active materials and the fused electrolyte, fluid mechanics plays a much larger role for LMBs than for most other battery types. Current densities routinely approach  $1 \text{ A/cm}^2$  and can be as high as  $13 \text{ A/cm}^2$ . The accompanying Joule heating is typically concentrated in the electrolyte layer. For many material combinations used in LMBs, the electrolyte's electrical conductivity is about four orders of magnitude lower than those of the electrodes, but see Fig. 3a for exceptions. This heat source in the middle of the cell will generally provide good mixing in the electrolyte and - depending on the height ratios - strong convection in the negative electrode [2]. Temperature gradients in the positive electrode should be stabilizing in most cases.

Current flow in batteries is accompanied and influenced by mass transport. This phenomenon is particularly pronounced in the positive electrode and is either generating or damping convection, depending on the current

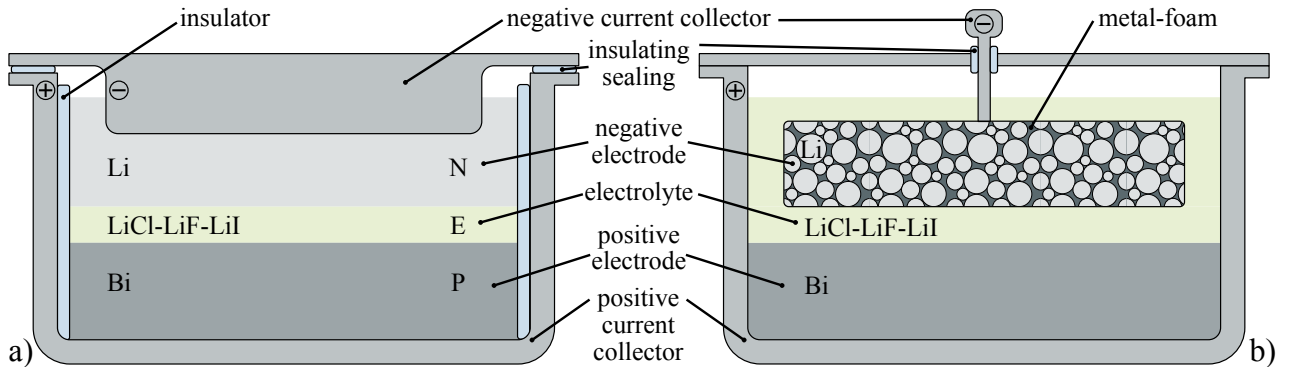


Figure 1: Sketch of liquid metal batteries implemented as a differential density cell (a) and a cell featuring a retainer (metal-foam in this case) for the negative electrode (b).

direction, see [3, 4] for examples. An estimation of the thermal and compositional Rayleigh numbers will typically predict a dominating solutal convection.

The high current density might as well give rise to electro-vortex flows as discussed in more detail in [5]. Their action could be beneficial, e.g., improving mixing in the positive electrode, but care should be taken to prevent disruptions of the electrolyte layer and to avoid resulting short circuits.

Preventing electrolyte layer disruptions is the main motivation for studying interfacial instabilities, the topic of the remainder of the present paper. A detailed discussion of the various driving forces for fluid motion in LMBs and consequences for their operation is provided in [6].

## 1 Sloshing in liquid metal batteries

The interfacial instability, which may occur in aluminum reduction cells is commonly known as “sloshing” or “metal pad roll instability”. Sele [7] suggested to use the ratio of Lorentz forces to gravity

$$\beta_{\text{Sele}} = \frac{I_c B_0}{g \Delta \rho h_{\text{Al}} h_{\text{cryolite}}} > \beta_{\text{crit}} \quad (1)$$

as a criterion for instability.  $B_0$  denotes a vertical magnetic field,  $g$  gravity,  $\Delta \rho$  the density difference between aluminum and cryolite, and  $h_{\text{Al}}$  and  $h_{\text{cryolite}}$  the layer heights of aluminum and cryolite, respectively. Naturally, only the horizontal components of the total cell current  $I_c$  are able to interact with the vertical magnetic field and Eq. (1) takes this into account.

Depending on the ratio of the density jumps at the two interfaces, Eq. (1) can give good predictions for instabilities in LMBs as well [8]. If the density jump at one interface is much smaller than that on the other, as is the case for the Mg|Sb LMB used in [8], the system can be described in good approximation as having an oscillating and a stationary interface. In this case, only the Mg|Electrolyte (N|E) interface is markedly deformed. Fig. 2b shows the ratio of the minimum electrolyte layer height to its initial value  $h_E/h_{E0}$  vs. a modified Sele parameter according to Eq. (6). This is Sele’s equation Eq. (1) supplemented by terms accounting for the conductivity differences and the interfacial tension. It is the latter that allows here for a better, but still imperfect collapse of the graphs compared to Fig. 12 of [8].

A system with a stationary and a moving interface is enforced as well in LMBs using a retainer for the negative electrode as sketched in Fig. 1b. Compared to aluminium reduction cells, tolerable electrolyte heights are limited to a few millimeters, typically  $h_E \leq 10$  mm since the open circuit voltage available for discharge does rarely exceed a value of 1 V.

If density jumps of comparable magnitude at both interfaces occur, the system dynamic becomes richer as described in [9]. However, not only the density ratios of the layers have an influence on the hydrodynamics but also the distribution of conductivities. This is the topic of the next section.

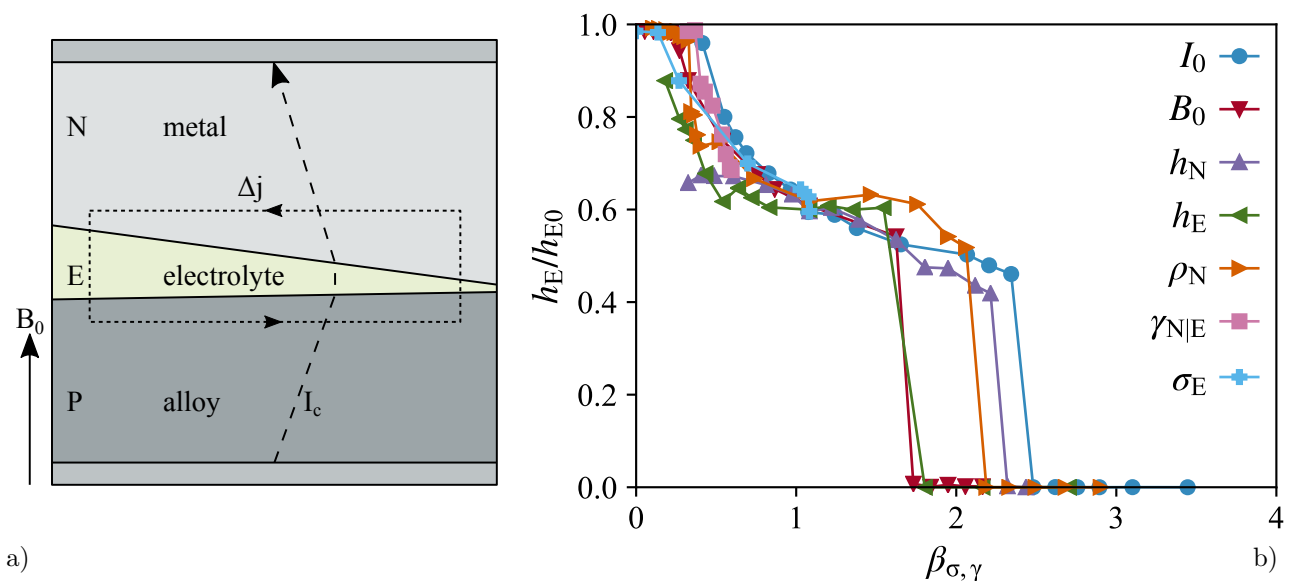


Figure 2: Sketch of the current path  $I_c$  and the compensation current  $\Delta j$  in a cell with tilted interfaces (a). Modified ratio of minimal to undisturbed electrolyte height  $h_E/h_{E0}$  vs. modified Sele parameter  $\beta_{\sigma,\gamma}$  according to Eq. (6) (b). Only the variable indicated in the legend is changed for each graph, all other values are kept constant.

## 2 Influence of the electrical conductivity distribution on sloshing

The distribution and strength of the compensation currents  $\Delta j$  sketched in Fig. 2a will depend on the conductivities of the three layers N, E, and P. Most, if not all, stability criteria developed for Hall-Héroult cells are rightly formulated without taking conductivities into account because the material system is quite fixed once and for all. This is not the case for LMBs, where several different material combinations are under investigation.

Starting from the assumption that the current in the low conducting electrolyte layer has to be a purely vertical one, the compensation current  $\Delta j$  in that layer can be modeled by starting from a series connection with a total area specific resistance  $R''_{\text{total}}$  given by

$$R''_{\text{total}} = R''_{\text{N}} + R''_{\text{E}} + R''_{\text{P}} = \frac{h_{\text{N}}}{\sigma_{\text{N}}} + \frac{h_{\text{E}}}{\sigma_{\text{E}}} + \frac{h_{\text{P}}}{\sigma_{\text{P}}} \quad (2)$$

with  $R''_i$ ,  $h_i$ ,  $\sigma_i$  denoting the area specific resistance, height, and conductivity of the three layers N, E, and P, respectively. By using the cell voltage to calculate the difference between horizontal and inclined interfaces while allowing only for small interface perturbations  $\eta_{\text{N|E}}$ ,  $\eta_{\text{E|P}}$ , one ends up with an expression for the compensation current in the hydrodynamic two-layer but electromagnetic three-layer case that is characteristic for the Mg||Sb cell:

$$\Delta j_{\text{N|E}} = -\frac{I_0(\sigma_{\text{E}} - \sigma_{\text{N}})\eta_{\text{N|E}}}{h_{\text{N}}\sigma_{\text{E}} + h_{\text{E}}\sigma_{\text{N}} + h_{\text{P}}\frac{\sigma_{\text{N}}\sigma_{\text{E}}}{\sigma_{\text{P}}}}. \quad (3)$$

From this perturbation current, a new Sele-like criterion can be formulated by relating the Lorentz forces to the balancing forces. Following [13], a Lorentz force scaling due to (3) results as:

$$F_{\text{L}} = \frac{(\sigma_{\text{N}} - \sigma_{\text{E}})I_0 B_0 \eta_{\text{N|E}}}{h_{\text{N}}(h_{\text{N}}\sigma_{\text{E}} + h_{\text{E}}\sigma_{\text{N}} + h_{\text{P}}\frac{\sigma_{\text{N}}\sigma_{\text{E}}}{\sigma_{\text{P}}})}. \quad (4)$$

Taking interfacial tension  $\gamma_{\text{N|E}}$  into account, the balancing forces scale as

$$F_{g,\gamma} = [(\rho_{\text{E}} - \rho_{\text{N}})g + \gamma_{\text{N|E}} \left(\frac{\epsilon_{mn}}{a}\right)^2] \eta_{\text{N|E}}, \quad (5)$$

cf. [9].  $\epsilon_{mn}$  marks the radial wavenumbers as described in [9], while  $a$  is the cell radius. In many cases the  $m = n = 1$  mode, giving  $\epsilon_{11} \approx 1.841$ , becomes most unstable to the metal pad roll instability. Taking the ratio of both forces from Eqs. (4) and (5) leads to a new stability criterion capturing the influence of the electrical conductivities as well as the interfacial tension:

$$\beta_{\sigma,\gamma} = \frac{(\sigma_{\text{N}} - \sigma_{\text{E}})I_0 B_0}{(h_{\text{N}}\sigma_{\text{E}} + h_{\text{E}}\sigma_{\text{N}} + h_{\text{P}}\frac{\sigma_{\text{N}}\sigma_{\text{E}}}{\sigma_{\text{P}}})h_{\text{N}}[(\rho_{\text{E}} - \rho_{\text{N}})g + \gamma_{\text{N|E}} \left(\frac{\epsilon_{mn}}{a}\right)^2]}. \quad (6)$$

Figure 3b shows  $\beta_{\sigma,\gamma}$  and the simplified version

$$\beta_{\text{Sele},\gamma} = \frac{I_0 B_0}{h_{\text{N}}h_{\text{E}}[(\rho_{\text{E}} - \rho_{\text{N}})g + \gamma_{\text{N|E}} \left(\frac{\epsilon_{mn}}{a}\right)^2]} \quad (7)$$

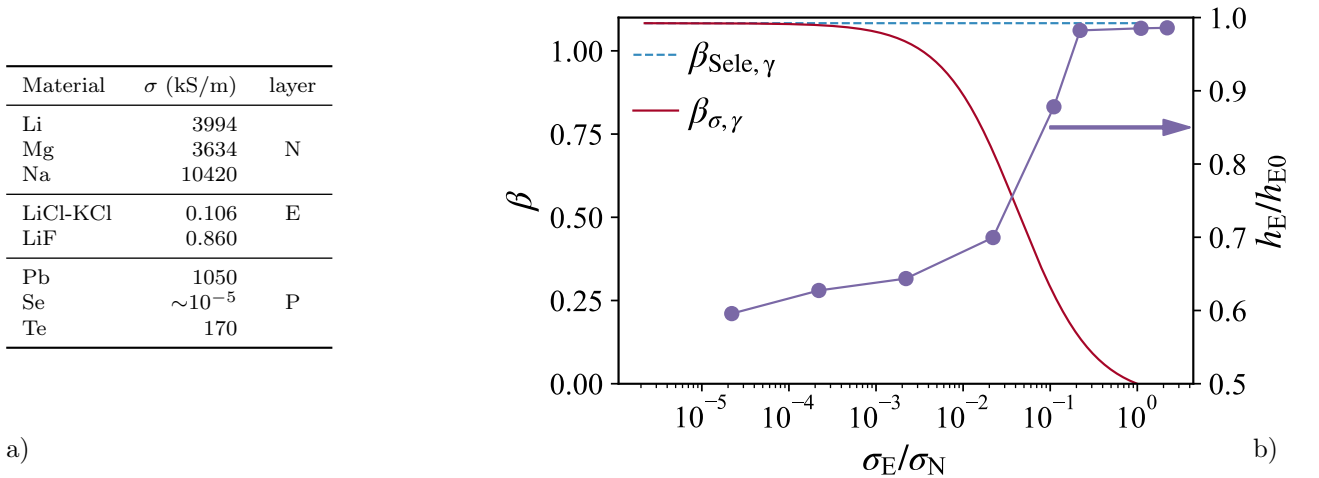


Figure 3: Conductivity values of selected active and electrolyte materials at melting point [6, 10], except Se  $\sigma(480^\circ\text{C})$  [11] and Te  $\sigma(452^\circ\text{C})$  [12] (a).  $\beta_{\text{Sele},\gamma}$  and  $\beta_{\sigma,\gamma}$  vs. conductivity ratio and corresponding interface deformation (b).

Table 1: Selection of binary alloy systems possessing a miscibility gap and approximate monotectic ( $T_m$ , melting temperature zinc in case of Na-Zn) and critical ( $T_K$ ) temperatures. The metals in the rows ‘upper layer’ and ‘lower layer’ are the main components of the alloys near  $T_m$  and  $\rho_{\text{upper}}$ ,  $\rho_{\text{lower}}$  the densities of the pure components at  $T_m$  (various sources).  $P$  and  $\sigma_{\text{upper}}/\sigma_{\text{lower}}$  denote the ultrasound reflectance and the ratio of conductivities, respectively, of the pure components at  $T_m$ . The higher  $P$ , the stronger is the reflection of an ultrasound beam incidenting perpendicularly to the interface.

lower layer	upper layer	$T_m$ °C	$T_K$ °C	$\rho_{\text{lower}}$ kg m <sup>-3</sup>	$\rho_{\text{upper}}$ kg m <sup>-3</sup>	$P$	$\frac{\sigma_{\text{upper}}}{\sigma_{\text{lower}}}$
Bi	Ga	222	258	10108	5992	0.00014	4.31
Bi	Zn	416	580	9879	6583	0.00492	3.69
Hg	Ga	27	204	13531	6102	0.00185	3.74
Pb	Ga	313	609	10689	5941	0.00415	3.02
Na	Li	171	303	911	515	0.00030	0.50
Zn	Na	420	819	6579	851	0.64974	1.64
Pb	Zn	420	802	10548	6579	0.00000	2.66
BiPb <sub>e</sub>	Ga	113	514	10566	6053	0.00078	3.99

in dependence on  $\sigma_E/\sigma_N$  using the standard case parameters from [8]. For  $\sigma_E/\sigma_N \lesssim 3 \cdot 10^{-4}$ ,  $\beta_\sigma$  is saturated and coincides with  $\beta_{\text{Sele}}$ . In that regime the assumption  $\sigma_E \ll \sigma_N$  is valid. In contrast, for  $\sigma_E/\sigma_N \gtrsim 3 \cdot 10^{-4}$ ,  $\beta_{\sigma,\gamma}$  is rapidly decreasing, meaning that destabilizing Lorentz forces decay and the system gets stabilized. The right ordinate of Fig. 3b displays numerical results for the minimal electrolyte layer height  $h_E$  relative to its initial value  $h_{E0}$  in dependence on  $\sigma_E/\sigma_N$ . These results show clearly that the decrease of  $\beta_{\sigma,\gamma}$  is indeed accompanied by a decline of the interface deformations and therefore a stabilization of the interface. Referring back, Fig. 2b contains data points for variations of the interfacial tension  $\gamma_{NE}$  and the conductivity  $\sigma_E$  with all other parameters kept at constant values. The corresponding data points fit quite well to the other curves supporting the initial assumptions.

Looking at the conductivity values in Tab. 3a, it becomes apparent that the electrical conductivities of the negative electrode and the electrolyte will probably fulfill the condition  $\sigma_N \gg \sigma_E$  in most cases, whereas the analogous requirement  $\sigma_P \gg \sigma_E$  is not always met. However, the latter finding will most likely not be of much practical relevance since both, tellurium as well as selenium, are very scarce goods and unlikely to be used at scale for LMBs. In addition, the conductivity of Se increases rapidly, if it is laced with highly conducting impurities, as is the case, e.g., in a Li|Se cell. Yet the above findings signal that one should take care when artificially reducing the conductivity differences between active materials and electrolyte in numerical LMB models [14]. In addition, it easily explains why model experiments using metal combinations with miscibility gaps (e.g., Li|Na, Ga|Pb, Bi|Ga, see table 1 for a selection) to study electromagnetically excited interfacial instabilities will face difficulties in achieving measurable interface deformations with moderate currents and magnetic fields.

### 3 Liquid metal two-layer systems

To quantify interface instabilities in liquid metal two layer systems, we discuss a few exemplary cases in the following. The forementioned difficulties notwithstanding, liquid metal systems possessing a miscibility gap have the advantage of easily supporting high current densities without associated chemical reactions since electrons are the charge carriers in both layers. These liquid metal systems might therefore be candidates for model experiments to study electromagnetically induced interface deformations. Besides the ratio of electrical conductivities, the densities and the acoustic properties of the pure components are listed in Tab. 1. Two immiscible liquids exist above the monotectic temperature ( $T_m$ , melting temperature zinc in case of Na-Zn) and below the critical temperature  $T_K$ , where the miscibility gap closes. An exemplary system with a miscibility gap is shown in Fig. 4a. The system consists of an eutectic Bi-Pb alloy (55.3-44.7 mol%) as the lower and Ga as the upper layer and is therefore a ternary one. The depicted isopleth is for the eutectic Bi-Pb composition, i.e.  $x_{\text{Pb}} = 0.808x_{\text{Bi}}$ . As a result, there is no well defined monotectic temperature at the Ga rich side, but probably a narrow mixed phase region. Detailed information could not be obtained by the simple cooling curve technique applied to generate the phase diagram. Besides this, the miscibility gap forms at relatively low temperature and persists for about 400 K. Interface detection by ultrasound would, however, be difficult because of the low reflectance of the interface. This property is shared by most of the listed systems except Na|Zn. The conductivity ratio of pure Ga to eutectic Bi-Pb is with almost 4 comparably high. It is outmatched only by Bi|Ga with 4.31. Experimentally, a conductivity ratio of about 2.5 can be measured at around 230 °C for Bi|Ga, because the conductivity contrast of the Bi-rich and Ga-rich phases existing in reality is lower than

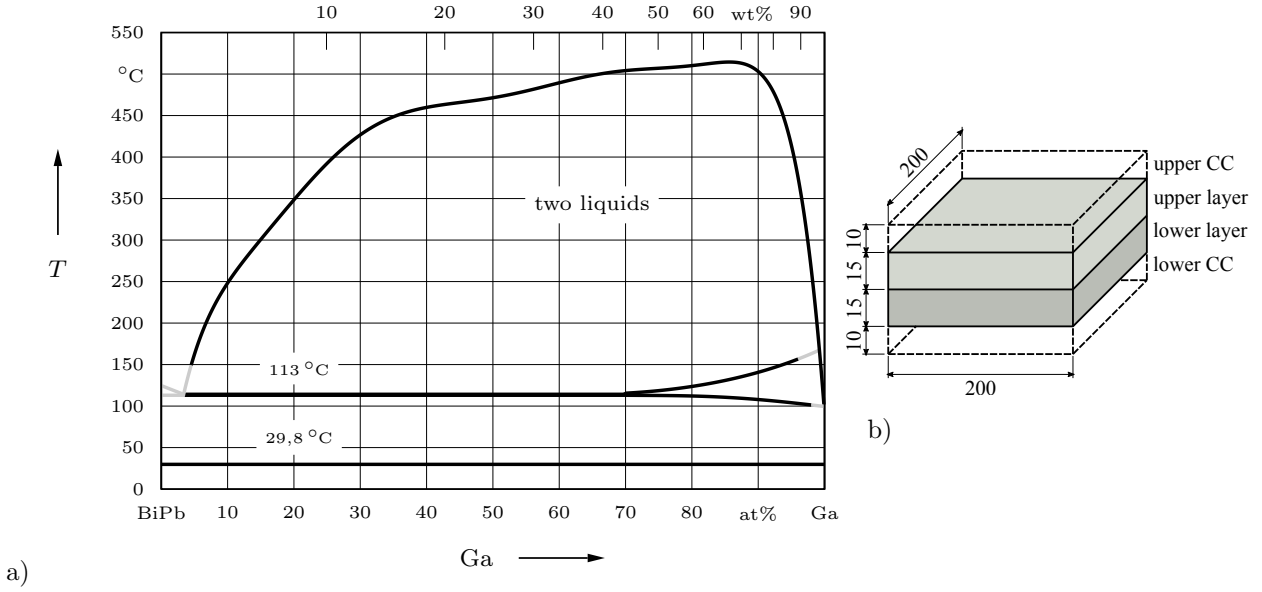


Figure 4: a) Experimental isopleth in the Bi-Ga-Pb system at  $x_{\text{Pb}} = 0.808x_{\text{Bi}}$  determined by simple cooling curves. b) sketch (not to scale, measures in mm) of the two layer arrangement. The depicted current collectors (CCs) were considered for a subset of the discussed cases only.

that of the pure components, especially for the relatively flat miscibility gap of the Bi-Ga system.

Excitation of interfacial waves by an externally applied vertical current in the presence of a vertical magnetic field was studied numerically with an OpenFOAM based solver using the volume of fluid method. Material properties of Bi-Ga at 222 °C are used for the simulations. Figure 4b displays a sketch of the geometry. Both liquid layers are 15 mm in height and have a cross section of  $200 \times 200 \text{ mm}^2$ . Current is applied to the top and the bottom surfaces. The setup is modeled with four different approximations: 1) Dirichlet boundary conditions directly at the liquids' surfaces (constant electric potential, DL), 2) Neumann boundary conditions directly at the liquids' surfaces (constant current, NL), 3) Dirichlet boundary conditions at the current collectors (DCC), and 4) Neumann boundary conditions at the current collectors (NCC).

In the first case (DL, Dirichlet b.c. at the liquids' surfaces), the first growing interfacial waves are detected for a critical current of  $I_{\text{cr}} = 3.78 \text{ kA}$  at an already quite strong magnetic field of  $B_z = 30 \text{ mT}$ . As can be seen in Fig. 5a), the growth rates increase linearly for  $I > I_{\text{cr}}$ . Fig. 5b) displays the growth rates of the waves for a constant current  $I = 3 \text{ kA}$  vs.  $B_z$ . This plot reveals that Fig. 5a) does not show the most critical instability. Instead  $B_z = 30 \text{ mT}$  is so high that it already damps waves that would occur for lower  $B_z$  and lower  $I$ . This behavior was recently found by Herreman et al. [15] for cylindrical reduction cells which give a more complete picture including stability curves in the  $I$ - $B_z$ -plane (Fig. 5 of [15]). The two cuts through this plane represented by Fig. 5a) and Fig. 5b) demonstrate that cells with square cross sections basically behave in a similar manner. Due to the high conductivities of both layers, the influence of magnetic damping on the waves is large and explains the decrease of the growth rates for  $B_z > 15 \text{ mT}$ .

Looking at the growth rates obtained with Neumann boundary conditions at the liquids' surfaces (second case, NL), a considerably lower critical current of  $I_{\text{cr}} = 2.2 \text{ kA}$  is observed and again a linear increase of the growth rate with the current. Correspondingly, wave damping in the NL case starts to decrease the growth rates later ( $B_z > 25 \text{ mT}$ ) and completely cancels them only at about  $B_z = 45 \text{ mT}$ . Neumann b.c. force the perturbation currents due to the interface inclination to close in the liquid layers, while Dirichlet b.c. do not impose such restrictions. Consequently, wave exciting Lorentz forces are stronger under Neumann b.c., resulting in lower critical currents, larger growth rates, and deferred overdamping.

Taking the current collectors (modeled with the conductivity of stainless steel that is slightly lower than that of the liquid metals) into account, changes especially the wave evolution for Dirichlet b.c. (DCC). The critical current for  $B_z = 30 \text{ mT}$  reduces to  $I_{\text{cr}} = 2.6 \text{ kA}$  and the growth rate increases almost in parallel with the Neumann b.c. cases. In Fig. 5b) damping decreases growth rates now for larger magnetic fields ( $B_z > 20 \text{ mT}$ ) compared to DL. This might be explained again by recurring to the horizontal perturbation currents. The lower conductivity of the current collectors effectively forces a larger part of the perturbation currents to close in the liquid metals. As mentioned before, Neumann b.c. maximize this effect, hence adding the current collectors to this case (NCC) does not markedly change the growth rates compared to the NL case.

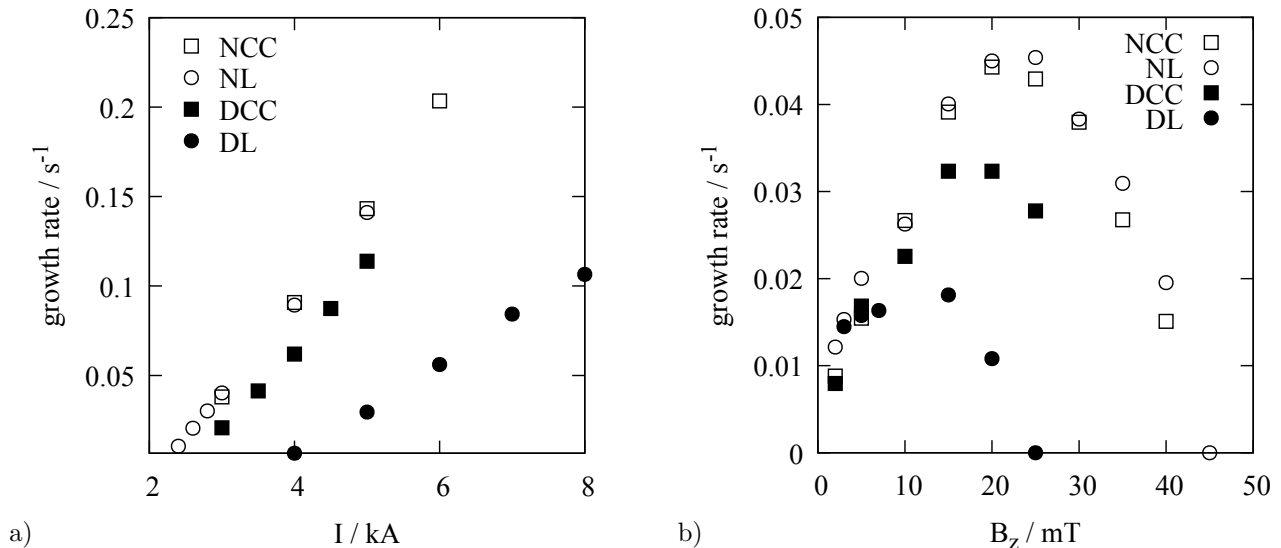


Figure 5: Growth rates of the interfacial waves for a constant  $B_z = 30$  mT vs. current (a) and for constant  $I = 3$  kA vs.  $B_z$  (b). NCC... Neumann b.c. at the current collectors, NL... Neumann b.c. at the liquids' surfaces, DCC... Dirichlet b.c. at the current collectors, DL... Dirichlet b.c. at the liquids' surfaces.

## 4 Conclusions

LMBs are electricity storage devices with a completely or dominantly liquid interior. Accordingly, fluid dynamics and magnetohydrodynamics are helpful in understanding and improving the operation characteristics of LMBs. Fluid flow can be generated by a number of mechanisms and may have different consequences. On the one hand, those can be beneficial as in the improved mixing inside the positive electrode that will foster capacity usage and prevent the growth of intermetallics. On the other hand, larger deformations of the interfaces should be avoided in order to keep the delicate electrolyte layer intact and thereby to avoid short-circuits.

Electromagnetically excited gravity waves may arise in the presence of a vertical magnetic field due to slight inclinations of the interface. The horizontal perturbation currents thereby evoked depend on the conductivities of the single layers. The lower the conductivity differences, the higher the critical current for wave amplification. A modified Sele parameter incorporating the conductivity ratios was proposed to take this effect into account.

Two layer liquid metal systems possessing a miscibility gap can be used to study interfacial wave dynamics in the lab. However, one has to resort to high electric currents and to cope with substantial magnetic damping. Boundary conditions have a marked influence on computed growth rates and the extension of the unstable region in the  $I$ - $B_z$ -plane.

## Acknowledgement

This work was supported by the Deutsche Forschungsgemeinschaft (DFG, German Research Foundation) by award number 338560565, by the Latvian Council of Sciences under project number lzp-2018/1-0017, and in frame of of the Helmholtz - RSF Joint Research Group "Magnetohydrodynamic instabilities: Crucial relevance for large scale liquid metal batteries and the sun-climate connection", contract No HRSF-0044 and RSF-18-41-06201. The computations were performed on the Bull HPC-Cluster "Taurus" at the Center for Information Services and High Performance Computing (ZIH) at TU Dresden and on the cluster "Hydra" at Helmholtz-Zentrum Dresden - Rossendorf. Fruitful discussions with Valdis Bojarevics, Wietze Herreman, Douglas Kelley, Caroline Nore, Donald Sadoway, and Oleg Zikanov on several aspects of metal pad roll instabilities and liquid metal batteries are gratefully acknowledged. N. Weber thanks Henrik Schulz for the HPC support.

## References

- [1] H. Kim, D.A. Boysen, J.M. Newhouse, B.L. Spatocco, B. Chung, P.J. Burke, D.J. Bradwell, K. Jiang, A.A. Tomaszowska, K. Wang, W. Wei, L.A. Ortiz, S.A. Barriga, S.M. Poizeau, and D.R. Sadoway. Liquid metal batteries: Past, present, and future. *Chem. Rev.*, 113:2075–2099, 2013.

- [2] Y. Shen and O. Zikanov. Thermal convection in a liquid metal battery. *Theor. Comput. Fluid Dyn.*, 30(4):275–294, 2016.
- [3] Paolo Personnettaz, Steffen Landgraf, Michael Nimtz, Norbert Weber, and Tom Weier. Mass transport induced asymmetry in charge/discharge behavior of liquid metal batteries. *Electrochemistry Communications*, 105:106496, 2019.
- [4] Paolo Personnettaz, Steffen Landgraf, Michael Nimtz, Norbert Weber, and Tom Weier. Effects of current distribution on mass transport in the positive electrode of a liquid metal battery. *Magnetohydrodynamics*, 56(2-3):247–254, 2020.
- [5] K. Liu, B. W. Li, F. Stefani, N. Weber, and T. Weier. Electro-vortex flow in a cylindrical container. In *Proc. 11<sup>th</sup> PAMIR Int. Conf. Fundamental and Applied MHD*, 2019.
- [6] Douglas H. Kelley and Tom Weier. Fluid mechanics of liquid metal batteries. *Applied Mechanics Reviews*, 70(2):020801, 2018.
- [7] T. Sele. Instabilities of the metal surface in electrolytic alumina reduction cells. *Met. Trans. B*, 8B:613–618, 1977.
- [8] N. Weber, P. Beckstein, W. Herreman, G. M. Horstmann, C. Nore, F. Stefani, and T. Weier. Sloshing instability and electrolyte layer rupture in liquid metal batteries. *Phys. Fluids*, 29:054101, 2017.
- [9] Gerrit Maik Horstmann, Norbert Weber, and Tom Weier. Coupling and stability of interfacial waves in liquid metal batteries. *J. Fluid Mech.*, 845:1–35, 2018.
- [10] P. Masset, A. Henry, J.-Y. Poinso, and J.-C. Poignet. Ionic conductivity measurements of molten iodide-based electrolytes. *J. Power Sources*, 160:752–757, 2006.
- [11] B. Lizell. The electrical conductivity of liquid selenium and selenium-tellurium mixtures. *The Journal of Chemical Physics*, 20(4):672–676, 1952.
- [12] J.C. Perron. Electrical and thermoelectrical properties of selenium-tellurium liquid alloys. *Advances in Physics*, 16(64):657–666, 1967.
- [13] Jean-Frédéric Gerbeau, Claude Le Bris, and Tony Lelièvre. *Mathematical Methods for the Magnetohydrodynamics of Liquid Metals*. Clarendon Press, 2006.
- [14] W. Herreman, C. Nore, L. Cappanera, and J.-L. Guermond. Tayler instability in liquid metal columns and liquid metal batteries. *J. Fluid Mech.*, 771:79–114, 2015.
- [15] W. Herreman, C. Nore, J.-L. Guermond, L. Cappanera, N. Weber, and G. M. Horstmann. Perturbation theory for metal pad roll instability in cylindrical reduction cells. *Journal of Fluid Mechanics*, 878:598–646, 2019.